

# Design and simulation of a novel method for determining depth-of-interaction in a PET scintillation crystal array using a single-ended readout by a multi-anode PMT

Mikiko Ito<sup>1</sup>, Jae Sung Lee<sup>2,3,4,5,7</sup>, Min-Jae Park<sup>2</sup>, Kwang-Souk Sim<sup>1</sup> and Seong Jong Hong<sup>6</sup>

<sup>1</sup> Department of Physics, Korea University, Seoul, Korea

<sup>2</sup> Department of Nuclear Medicine, Seoul National University, Seoul, Korea

<sup>3</sup> Department of Biomedical Sciences, Seoul National University, Seoul, Korea

<sup>4</sup> Department of Brain and Cognitive Sciences, Seoul National University, Seoul, Korea

<sup>5</sup> Department of Institute of Radiation Medicine, Seoul National University, Seoul, Korea

<sup>6</sup> Department of Radiological Science, Eulji University, Gyeonggi-do, Korea

E-mail: [jaes@snu.ac.kr](mailto:jaes@snu.ac.kr)

Received 12 August 2009, in final form 11 May 2010

Published 15 June 2010

Online at [stacks.iop.org/PMB/55/3827](http://stacks.iop.org/PMB/55/3827)

## Abstract

PET detectors with depth-of-interaction (DOI) encoding capability allow high spatial resolution and high sensitivity to be achieved simultaneously. To obtain DOI information from a mono-layer array of scintillation crystals using a single-ended readout, the authors devised a method based on light spreading within a crystal array and performed Monte Carlo simulations with individual scintillation photon tracking to prove the concept. A scintillation crystal array model was constructed using a grid method. Conventional grids are constructed using comb-shaped reflector strips with rectangular teeth to isolate scintillation crystals optically. However, the authors propose the use of triangularly shaped teeth, such that scintillation photons spread only in the  $x$ -direction in the upper halves of crystals and in the  $y$ -direction in lower halves. DOI positions can be estimated by considering the extent of two-dimensional light dispersion, which can be determined from the multiple anode outputs of a position-sensitive PMT placed under the crystal array. In the main simulation, a crystal block consisting of a  $29 \times 29$  array of  $1.5 \text{ mm} \times 1.5 \text{ mm} \times 20 \text{ mm}$  crystals and a multi-anode PMT with  $16 \times 16$  pixels were used. The effects of crystal size and non-uniform PMT output gain were also explored by simulation. The DOI resolution estimated for  $1.5 \times 1.5 \times 20 \text{ mm}^3$  crystals was 2.16 mm on average. Although the flood map was depth dependent, each crystal was well identified at all depths when a corner of the crystal array was irradiated with 511 keV gamma rays (peak-to-valley ratio  $\sim 9:1$ ). DOI resolution was better than

<sup>7</sup> Author to whom any correspondence should be addressed.

3 mm up to a crystal length of 28 mm with a  $1.5 \times 1.5 \text{ mm}^2$  or  $2.0 \times 2.0 \text{ mm}^2$  crystal surface area. The devised light-sharing method allowed excellent DOI resolutions to be obtained without the use of dual-ended readout or multiple crystal arrays.

## 1. Introduction

In the high-resolution positron emission tomography (PET) systems used to image small animals or specific organs, the diameter of the detector ring and the cross-sectional areas of individual scintillation crystal elements should be small enough to enhance sensitivity and spatial resolution, whereas the crystal length should be long enough to enhance 511 keV gamma ray detection efficiency. However, the spatial resolutions of these small ring scanners degrade rapidly in the peripheral region of the field of view (FOV), due to ‘parallax errors’ caused by obliquely incident gamma rays (Derenzo *et al* 1989, Moses 2001) if the depth-of-interaction (DOI) of a gamma ray within the crystal is unknown (parallax errors cause radial elongation artifact at the FOV periphery (Kim *et al* 2007, Visser *et al* 2009)). Therefore, DOI determination within crystals to achieve high spatial resolution and high sensitivity, without causing deterioration in spatial resolution uniformity, is one of the most active PET development topics (Lewellen 2008).

One of the most investigated DOI estimation methods involves the use of multiple layer scintillation crystals, which have the different characteristics in terms of scintillation decay time, relative position offset between crystal layers and arrangements of reflectors between crystals (Seidel *et al* 1999, Streun *et al* 2003, Wang *et al* 2006, Zhang *et al* 2003, Orita *et al* 2005, Hong *et al* 2008). However, these methods provide only discrete DOI information, which is limited by the number of layers, and typically ranges from 5 to 10 mm (Lewellen 2008, Yang *et al* 2008). Light losses between layers and costs versus mono-layer crystal designs are also drawbacks of these multiple layer-based methods.

Accordingly, a method such as continuous DOI determination is required. One approach to continuous DOI determination involves the use of dual-ended crystal readout. This method employs two photosensors at crystal ends to measure scintillation light output and determines DOI location by comparing light outputs, because more light is detected when a photosensor is closer to the DOI (Moses *et al* 1995, Shao *et al* 2000). Recent reports have shown that DOI resolutions of 2 mm can be achieved using this approach (Abreu *et al* 2006, Yang *et al* 2008). A different dual-ended readout scheme has also been investigated using a monolithic crystal block (Maas *et al* 2009).

However, additional expensive solid-state photosensors and compact ASIC front-end electronics are required to measure light output from the front surfaces of crystal to minimize gamma ray attenuation and scattering. Radiation damage to solid-state photosensors and electronics by gamma rays is also a matter of concern, and the reduction of dead space between detector modules is technically challenging (Shao *et al* 2000).

The aim of this work was to develop a DOI encoding method for a mono-layer scintillation crystal array with a single-ended readout using a multi-anode photomultiplier tube (PMT) or a solid-state photosensor array. Our method is based on the spreading of light within a crystal array via reflectors that partially cover the crystal surfaces, as illustrated in figure 1(a). DOIs were determined by measuring the two-dimensional (2D) dispersion of light from the single end of a crystal array. In this paper, we describe the concept underlying our approach and detector module performances estimated by Monte Carlo simulation.

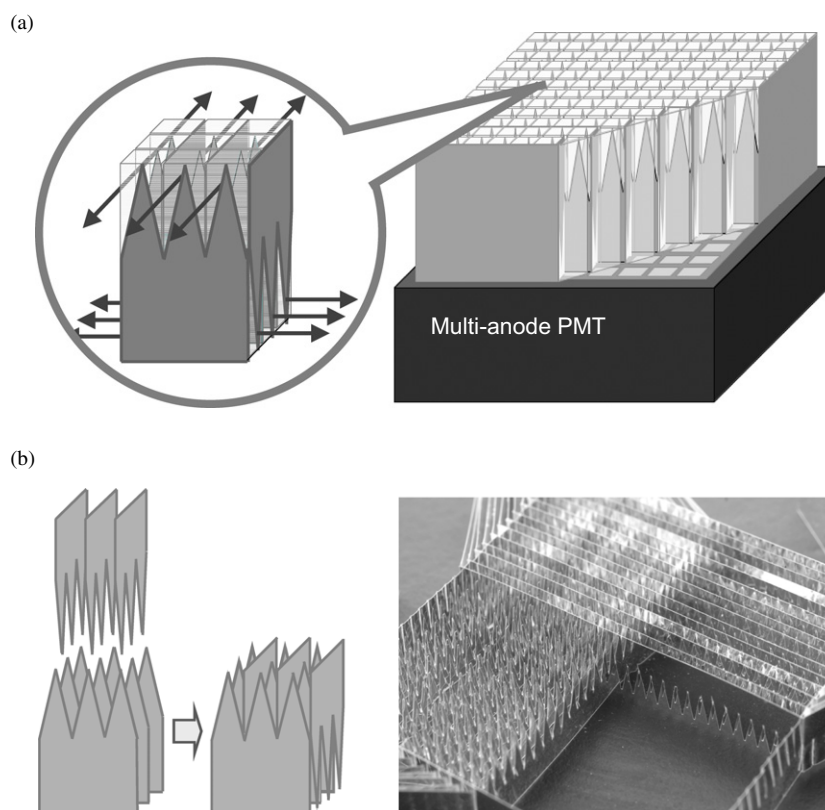


**Figure 1.** DOI-encoding detector composed of a mono-layer crystal block and a single-ended readout scheme: (a) detector module and (b) reflector grid structure utilized in the proposed light spreading method for DOI encoding.

## 2. Materials and methods

### 2.1. Light spreading method

In a typical crystal array, individual crystals are separated by a reflective grid composed of crossed comb-shaped reflector strips, to ensure that individual crystal elements are optically isolated (Miyaoka *et al* 2001). In the conventional grid method, each reflector strip has rectangular teeth, which locate in gaps between teeth on orthogonally disposed strips.

In our light spreading method, triangular teeth are used, rather than rectangular teeth, to allow scintillation photons to spread across crystals. Figure 1(b) shows how a reflector grid is constructed with these modified strips. When these strips are used, the surfaces of crystals are partly uncovered by the reflector strips and optical crosstalk occurs via these uncovered regions. Using this design, the directions and extents of light spread in the  $x$ - and  $y$ -directions are dependent on DOI within the crystal array, as scintillation photons can travel only in the  $x$ -direction in the upper half of the array and only in the  $y$ -direction in lower half (figure 1(a)). Uncovered areas in the  $x$ - and  $y$ -directions also depend on the crystal length because of the triangular teeth. Hence, DOI positions can be estimated from the 2D variances

**Table 1.** Configurations of crystal blocks used in simulations to examine the relation between crystal size and DOI resolution. Crystal lengths varied between 12 and 28 mm.

Crystal cross-sectional area (mm × mm)	Array size ( $n \times n$ )	Crystal pitch (mm)	Total block area (mm × mm)
1.0 × 1.0	42 × 42	1.1	46.1 × 46.1
1.5 × 1.5	29 × 29	1.6	46.3 × 46.3
2.0 × 2.0	22 × 22	2.1	46.1 × 46.1

of signal outputs from the anode array of a position-sensitive PMT or a solid-state photosensor array.

## 2.2. Detector design and simulation

The GATE Monte Carlo simulation toolkit (Jan *et al* 2004) was used to investigate the performance of the detector module. The designed detector module is composed of a single-layer crystal array and a multi-anode flat panel PMT, which we also used in our previous studies (Hong *et al* 2008, Kwon *et al* 2008). The crystal array consists of LSO (lutetium oxyorthosilicate;  $\text{Lu}_2\text{SiO}_5$ ,  $7.4 \text{ g cm}^{-3}$ ) crystals. To examine dependence of DOI resolution on crystal size, we tested various arrays of crystals with different crystal lengths (12, 16, 20, 24 and 28 mm) and cross-sectional areas ( $1.0 \times 1.0 \text{ mm}^2$ ,  $1.5 \times 1.5 \text{ mm}^2$  and  $2.0 \times 2.0 \text{ mm}^2$ ). The configurations of crystal blocks simulated are summarized in table 1. Both polished and unpolished crystal arrays were investigated. Crystal arrays were optically coupled to a multi-anode PMT using optical grease. The PMT simulated had 256 ( $16 \times 16$  array) sensitive pixels and a pitch of 3.04 mm (total sensitive area =  $49 \times 49 \text{ mm}^2$ ) (this configuration is the same as that used in the Hamamatsu H9500 PMT).

While the typical light yield of LSO is  $26\,000 \text{ photons MeV}^{-1}$ , we assigned a light yield of  $6240 \text{ photons MeV}^{-1}$  for LSO by assuming a 24% quantum efficiency (QE) of the H9500 PMT in advance. In GATE, the number of photons emitted per amount of absorbed energy follows a normal distribution. The standard deviation of this normal distribution relative to energy resolution is determined by the ‘resolution scale’ and light yield of the crystal (GATE users guide). We chose the ‘resolution scale’ of LSO by assuming an energy resolution of 16% with a light yield of  $6240 \text{ photons MeV}^{-1}$ .

The reflector polymer has a thickness of 0.065 mm, and the PMT entrance window consists of glass of density  $2.5 \text{ g cm}^{-3}$ . The thickness of the PMT window is 1.5 mm as mentioned in the H9500 PMT datasheet. A grease ( $\text{C}_1\text{H}_1\text{O}_1$ ,  $1.0 \text{ g cm}^{-3}$ ) layer of thickness 0.1 mm is present between the crystal array and PMT entrance window (van der Laan *et al* 2010). Because a crystal pitch is 0.1 mm larger than the crystal surface size, a 0.1 mm space is located between crystals. A reflector of thickness 0.065 mm with a triangular toothed shape was placed in the center of this space. Because the reflector was partially placed between crystals due to the shape, a gap of 0.0175 mm exists between the crystal and the reflector, and a gap of 0.1 mm between crystals in the absence of the reflector. All gaps were air filled.

GATE tracks the propagation of individual light photons inside the detector module. During the GATE optical simulation, photon interactions at boundaries between media were described using the UNIFIED model (GATE users guide; Levin and Moisan 1996, van der Laan *et al* 2010). On the surface of the reflector, it was assumed that photons are reflected with a reflectivity of 98% using the ‘Paint’ model. We defined the other surfaces using the ‘Ground’ model, between the crystal and grease, grease and PMT window, and the crystal and air gap.

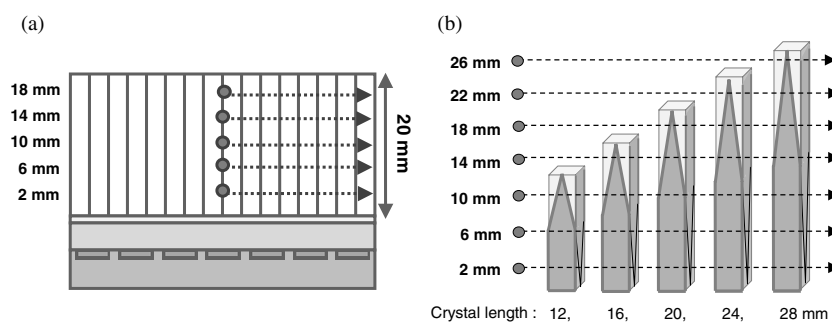


**Figure 2.** Gamma ray pencil beam radiation (a) to estimate DOI resolution in  $1.5 \times 1.5 \times 20 \text{ mm}^3$  crystals and (b) to examine the relation between the crystal size and DOI resolution.

On these surfaces, when a scintillation photon reaches the surface between two materials, it is either reflected or refracted with a probability determined by the angle of incidence and the refractive indices of the two materials. We used refractive indexes of 1.82, 1.5 and 1.5 for the LSO crystals, grease and PMT entrance window, respectively.

In the ‘Ground’ model, the roughnesses of these surfaces were modeled as if they were composed of small micro facets. These surface variations were described using ‘sigma-alpha’ values (standard deviations of alpha values), where alpha (random angle) is the angle between the micro facet normal and average surface normal.

Sigma-alpha values were directly measured by scanning the crystal surface by atomic force microscopy. Sampled surface height distribution was differentiated in steps of  $\sim 2 \mu\text{m}$  to obtain the distribution of micro-facet slopes, referred to as ‘alpha’, as described in Levin and Moisan (1996). The standard deviation of the distribution of alpha (sigma-alpha) indicates surface roughness. We obtained sigma-alpha values of 5.6 for an unpolished crystal surface and  $\sim 0.0$  for a polished crystal surface. Since a sigma-alpha value of 0.0 means a perfect-specular surface, we assigned a sigma-alpha of 0.1 instead of 0.0 to a polished surface and PMT entrance window (glass).

Behind the PMT window, sensitive pixels (photocathodes) were arranged in a  $16 \times 16$  array. All optical photons that reached sensitive pixels were detected. While sensitive pixels had an efficiency of 100%, this simulation included the effect of QE, because the light yield was modified to consider the QE of the photocathode. It provides the definite advantage of reducing simulation time because the number of light photons to be tracked is reduced. However, we did not incorporate PMT dark current, excess noise, or readout electronics noise in the simulation.

### 2.3. DOI estimations

DOI resolutions were estimated using gamma ray sources with a mono-energy of 511 keV. The crystal array was irradiated with a pencil beam of gamma rays at 4 mm intervals (2, 6, 10, 14, 18, 22 and 26 mm deep from the PMT surface) to examine DOI-encoding capability, as shown in figure 2.

We estimated DOI positions based on the variances (squares of standard deviations) of numbers of detected photons at the sensitive-pixel array, taking into account QE as explained above (refer to section 3 for details). Variances in  $x$ - and  $y$ -directions were calculated using

$$\sigma_x^2 = \frac{\sum_i (x_i - x_0)^2 \times N_i}{\sum_i N_i} \quad (1a)$$

$$\sigma_y^2 = \frac{\sum_i (y_i - y_0)^2 \times N_i}{\sum_i N_i}, \quad (1b)$$

where  $x_i$  and  $y_i$  are the  $x$  and  $y$  positions (center) of each sensitive pixel of the PMT, respectively,  $N_i$  is the number of photons detected per pixel and  $x_0$  and  $y_0$  are the mean values of  $x_i$  and  $y_i$  weighted by  $N_i$ . 2D flood images (the histograms of  $x_0$  and  $y_0$ ) were also composed.

#### 2.4. Generation of flood maps

In addition, a cone-beam gamma ray source was located 10 cm away from the front surface of the center crystal in a  $5 \times 5$  array located at the corner of a crystal block consisting of a  $29 \times 29$  array of  $1.5 \text{ mm} \times 1.5 \text{ mm} \times 20 \text{ mm}$  crystals. The opening angle of the cone-beam source was  $3.5^\circ$ . The aim of this ‘front on’ irradiation was to explore possible flood image distortion due to different light dispersion patterns depending on the DOI position and to find a way of identifying correct crystal positions. We only focused on the corner crystal block because asymmetrical light dispersion in this area is the possible source of the DOI-dependent centroid shift. This shift was ignorable in the center of the crystal block because light dispersion is symmetrical in this area.

#### 2.5. Effects of non-uniform gain of PMT output

The DOI estimation accuracy of the present approach is likely to be sensitive to gain non-uniformity in a multi-anode PMT, because this approach estimates 3D event position based on the light response function across the full sensitive area of the multi-anode PMT. To examine the effects of such non-uniform gain of PMT output on DOI estimation, we included the gain map of a representative H9500 PMT in the simulation.

### 3. Results

#### 3.1. DOI determinations

DOI responses were determined by simulation for both the polished and unpolished crystal arrays. We found DOI dependence of light dispersion only for unpolished crystals, and therefore, all results given here were obtained using these crystals.

Figure 3(a) shows 2D variances obtained using a  $1.5 \times 1.5 \times 20 \text{ mm}^3$  crystal array. The red, yellow, blue, green and brown points in the figure indicate events that occurred after gamma-beam irradiation at 2, 6, 10, 14 and 18 mm, respectively, from the border of the crystal array and the multi-anode PMT. Because light spreading in the lower half of the crystal array is allowed only in the  $y$ -direction and decreases with distance from the PMT surface, events at the 2, 6 and 10 mm DOI positions have different  $y$ -variances. Using the same principles for light spread in the upper halves of crystals, events at the 10, 14 and 18 mm DOI positions were found to have different  $x$ -variances.

For each data point, the difference between  $x$ - and  $y$ -variances ( $\sigma_x^2 - \sigma_y^2$ ) was calculated, and these differences were regarded as indices of the DOI position. Figure 3(b) shows a histogram for  $\sigma_x^2 - \sigma_y^2$  in which peaks for all DOI positions are clearly separated. Peak positions in the  $\sigma_x^2 - \sigma_y^2$  distribution were calibrated to the irradiation positions (DOI positions), and the average full width at half maximum (FWHM) of the peaks was calculated to estimate the

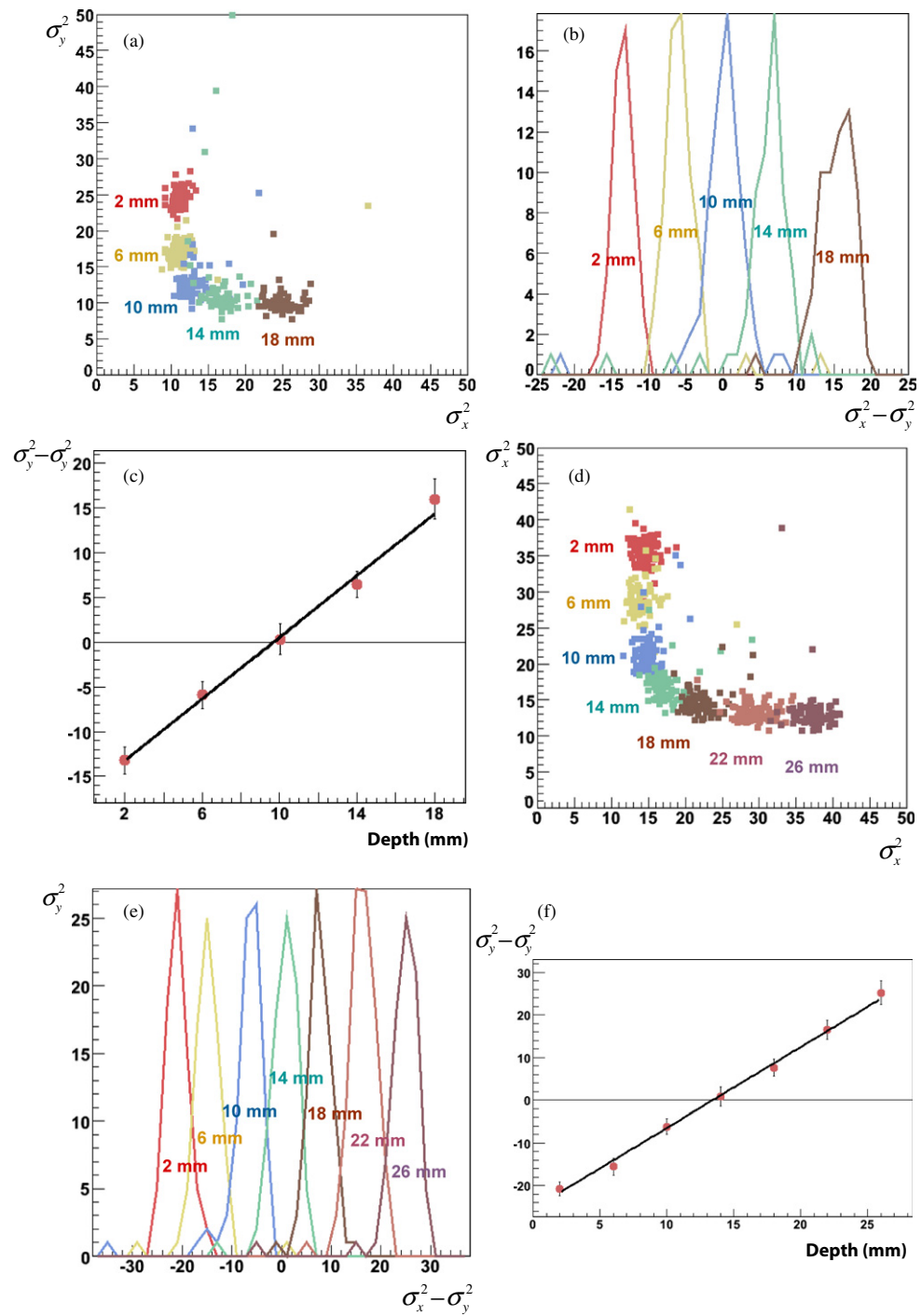


**Figure 3.** DOI estimation based on light dispersion: (a) 2D variance map, (b)  $\sigma_x^2 - \sigma_y^2$  histograms and (c) relationship between  $\sigma_x^2 - \sigma_y^2$  and DOI position obtained by irradiating five different positions with collimated gamma rays at 4 mm intervals within an array of discrete crystals of dimension  $1.5 \times 1.5 \times 20 \text{ mm}^3$ . (d)–(e) The same data for  $2.0 \times 2.0 \times 28 \text{ mm}^3$  crystals.

DOI resolution using the calibration that substitutes 4 mm for the average distance between the  $\sigma_x^2$ - $\sigma_y^2$  peaks. The DOI resolution is estimated to be 2.16 mm for a  $1.5 \times 1.5 \times 20$  mm<sup>3</sup> crystal array.

Figure 3(c) shows that an excellent linear relationship with the DOI position is obtained. Figures 3(d)–(f) show the 2D variance map, the  $\sigma_x^2$ - $\sigma_y^2$  histogram and the  $\sigma_x^2$ - $\sigma_y^2$  versus DOI relationship for the crystal of  $2.0 \times 2.0 \times 28$  mm<sup>3</sup>, which yields a DOI resolution of 2.63 mm.

### 3.2. Crystal identification

In the proposed crystal array, the direction and extent of scintillation photon dispersion depend on the DOI position. This DOI-dependent photon dispersion causes a blurring of flood images near the edge of the crystal array, because in this area, the peak position of each crystal is shifted inward the block due to a high level of light reflection and light loss at the end of the array. The amount of the positional shift is proportional to the extent of light spreading at each DOI position. Therefore, we propose the composition of different flood maps for quantized different DOI positions to achieve proper crystal identification.

Figure 4(a) shows a density plot of  $x$ - and  $y$ -variances of the photon distribution on the pixel array of the PMT after irradiating the corner of the crystal array ( $29 \times 29$  array of  $1.5$  mm  $\times$   $1.5$  mm  $\times$   $20$  mm crystals) with cone-beam gamma rays. A continuous distribution of data points for different DOI positions is observed. The upper row of figure 4(b) shows flood maps for events that occurred at five different interaction depths and indicates that all  $5 \times 5$  crystals at array corners are clearly separated by depth-dependent crystal identification. The average peak-to-valley ratio in the  $x$ - and  $y$ -projections (middle and lower rows in figure 4(b)) is  $\sim 9:1$ . As was expected, peaks in flood images are broader in the  $y$ -direction for the lower half of the array, and in the  $x$ -direction for the upper half of the array.

### 3.3. Effects of crystal size on DOI resolution

DOI resolution depends on crystal dimensions, perhaps because differences in light dispersion are determined by crystal size. The cross-sectional areas and lengths of crystals are related to the widths and lengths of crystal side surfaces not covered by the reflector grid, and this causes light to spread through the crystal array.

DOI resolutions estimated for various crystal dimensions, that is, three surface sizes ( $1.0 \times 1.0$ ,  $1.5 \times 1.5$  and  $2.0 \times 2.0$  mm<sup>2</sup>) and five crystal lengths (12, 16, 20, 24 and 28 mm) are shown in figure 5, which shows average values of DOI resolutions over all irradiated depth positions for the center crystal in an array. Because the crystal length is a principal determinant of the intrinsic detection efficiency of gamma rays, a crystal length should be chosen after considering the tradeoff between DOI resolution and detection efficiency.

Figure 6 shows 2D variance maps for all combinations of surface sizes and crystal lengths.

### 3.4. Effects of non-uniform gain of PMT output

In figure 7, DOI responses obtained at the center of crystal array without and with incorporating the gain non-uniformity of the anode in multi-anode PMT are compared (all the results previously shown were obtained assuming uniform PMT gains). Figure 7(a) shows the anode uniformity map of a representative H9500 PMT incorporated in the simulation. Although the 2D variances are distorted by gain non-uniformity, the basic tendency of DOI response is not

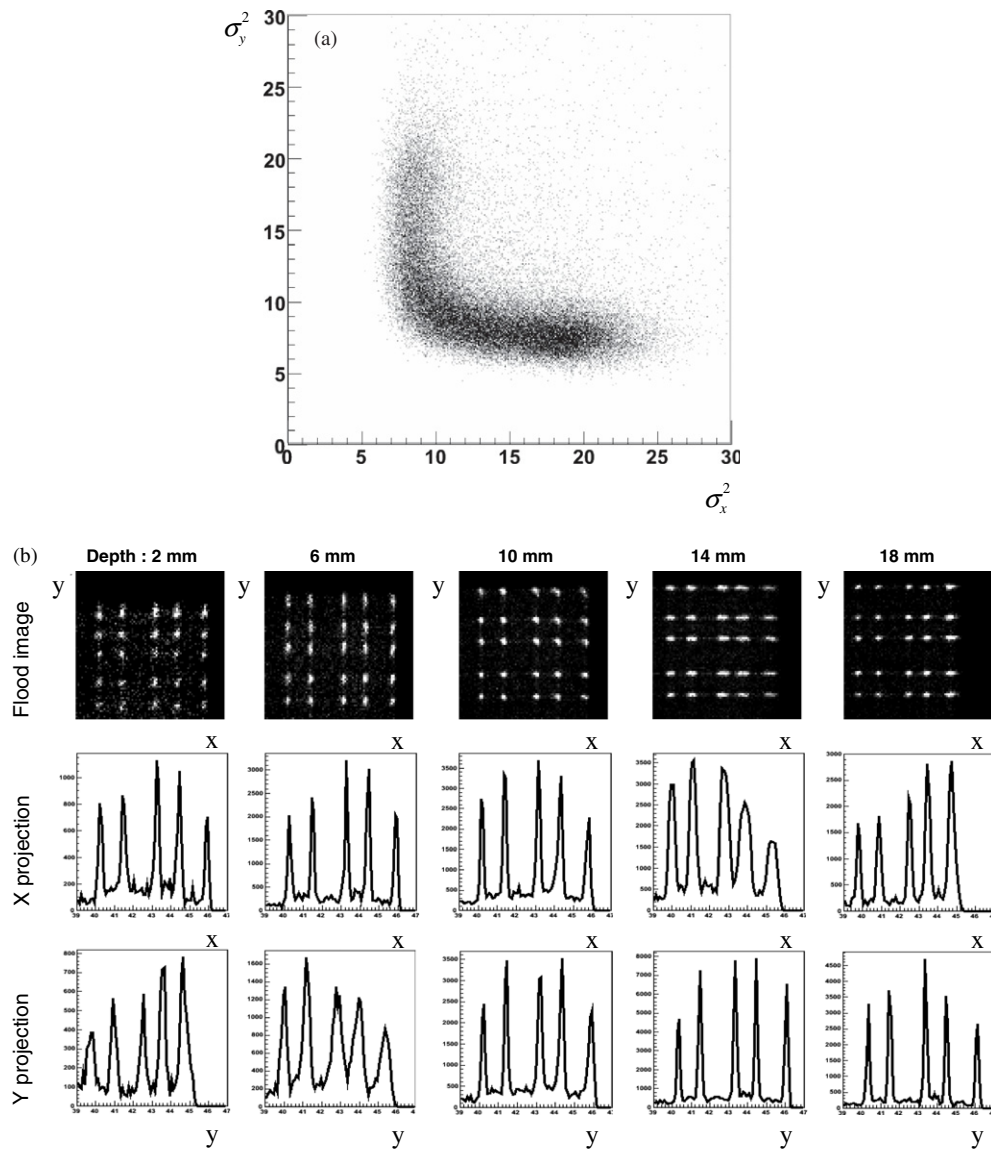


**Figure 4.** Depth-dependent crystal identification at the corner of the crystal array. (a) 2D variance map and (b) flood histograms (upper row) at five different DOI positions obtained when the corner of the crystal array ( $29 \times 29$  array of  $1.5 \text{ mm} \times 1.5 \text{ mm} \times 20 \text{ mm}$  crystals) was exposed to cone-beam gamma rays and their projection profiles in the  $x$ - and  $y$ -directions (middle and lower rows).

changed and DOI positions are still distinguishable in the variance maps (figure 7(b) versus figure 7(c)).

However, this result suggests that gain non-uniformity results in different DOI responses along the crystal positions within a crystal array, and that PMTs with different gain distributions would lead to different DOI responses. Accordingly, the use of a delicate compensation method to adjust for gain non-uniformity, such as that described by Popov *et al* (2006), will be necessary when this approach is implemented in real situations.

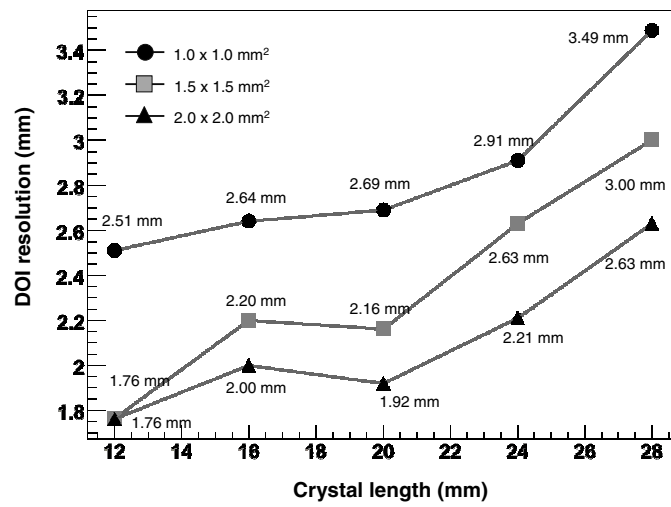


**Figure 5.** Effects of crystal size on DOI resolution. DOI resolution for various crystal sizes, that is, three cross-sectional areas ( $1.0 \times 1.0$ ,  $1.5 \times 1.5$  and  $2.0 \times 2.0$  mm<sup>2</sup>) and five crystal lengths (12, 16, 20, 24 and 28 mm).

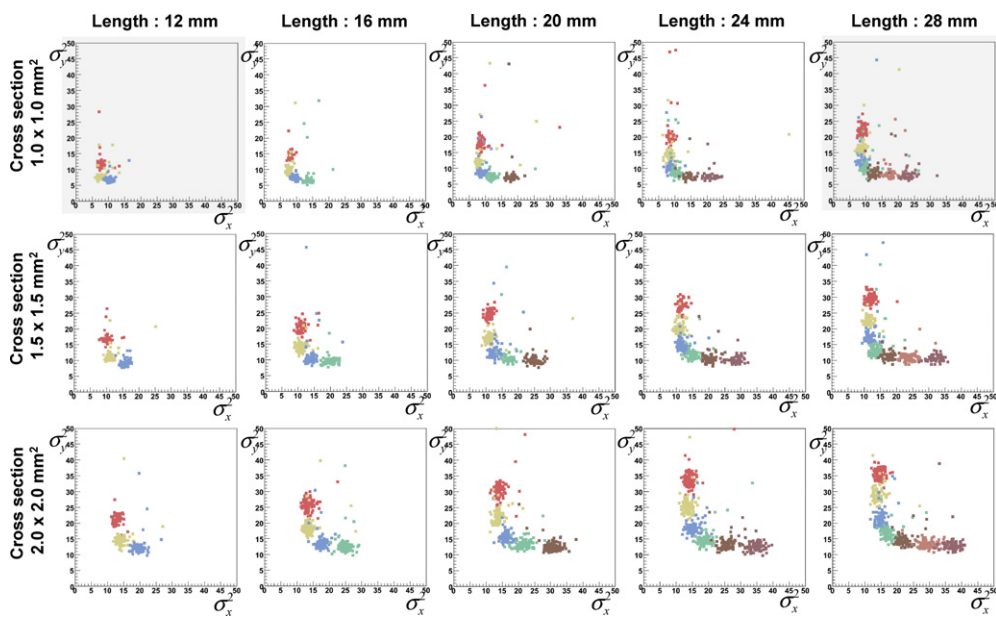


**Figure 6.** 2D variance maps for the crystal size detailed in figure 5.

#### 4. Discussion

Cost effectiveness is one of the most important issues of DOI-encoding PET detector development, especially, the costs of photosensors and scintillation crystals. In terms of

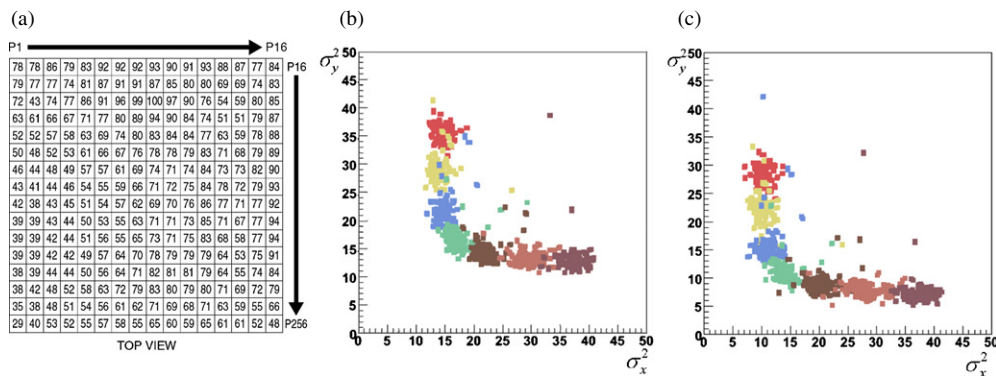


**Figure 7.** Effects of non-uniform gain of PMT output on DOI response. (a) Anode uniformity map of a representative multi-anode PMT (H9500). (b) 2D variance map obtained without incorporating gain non-uniformity. (c) 2D variance map obtained after incorporating gain non-uniformity.

function, output channel density is critical when building a full-ring detector with a sufficient axial FOV.

In order to develop a cost-effective DOI-encoding PET detector, several DOI estimation methods have been proposed for a mono-layer crystal block with a single-ended readout. One of the earliest proposed designs (the dMiCE detector) was based on an array of two-crystal pairs with a triangular reflector placed between crystal pairs that allowed them to share scintillation light (Miyaoaka and Lewellen 1998, Lewellen *et al* 2003). In this design, the DOI position was determined by calculating the ratio of light outputs from crystal pairs. Although the basic concept of our design is similar to that of the dMiCE detector, the DOI resolution of our approach should be much better, because the upper and lower halves of the crystal arrays spread light in different directions, and 2D spreading is used instead of the one-dimensional sharing used in dMiCE.

In the early dMiCE design, a multi-anode PMT was used as a single-ended readout device, and paired crystals were connected to different pixels in the PMT to allow individual light outputs from crystal pairs to be measured. Therefore, the cross-sectional areas of crystals should be matched with the sizes of sensitive pixels in the PMT, which reduces the flexibility of the detector design. The dMiCE design also suffered from DOI-response deterioration due to light dispersion between the PMT surface and its sensors, even though crystal pairs were coupled accurately to PMT pixels. To solve these problems, a detector modification was suggested, whereby individual crystals were directly coupled with a micropixel avalanche photodiode instead of a multi-anode PMT. In addition, DOI accuracy was improved by estimating the first event position of a multiple interaction within the crystal array using a statistical positioning algorithm (Champley *et al* 2008). The DOI resolution achieved to date using this approach is about 3–4 mm (Lewellen *et al* 2003), but a large number of solid-state photosensors and readout electronics would be required to build the detector modules. In contrast, our method requires only a multi-anode PMT connected to an analog circuit modified from a widely used charge division circuit to calculate centroids and variances of light distributions simultaneously (Lerche *et al* 2009). The circuit devised by Lerche *et al* (2009) is simple to implement because only the resistor chains and OP amps are required in the circuit. However, some modification of the circuit is needed to obtain the  $x$ - and  $y$ -variances required by our method, because Lerche's circuit only provides one-dimensional variance of light distribution based on an assumption of isotropic symmetry.

Other single-ended readout detectors consist of a mono-layer phosphor-coated crystal array and estimate DOI using the pulse shape discrimination (PSD) method (Du *et al* 2009). This design utilizes ‘phosphor’ to modify the decay time of scintillation light instead of multi-layered crystals with different decay constants as are used in the conventional PSD design. In this detector, the upper halves of LSO crystals were coated with a thin layer of phosphor, which absorbs some fraction of LSO scintillation light (decay time: 40 ns) and re-emits the light with a decay time of 70 ns. Since the amount of light that reaches the phosphor depends on the DOI position, DOI information can be extracted from LSO scintillation to re-emitted light ratios (Lewellen *et al* 2003). The detector module uses two charge integration windows to measure light amounts during the early and delayed portions of the output pulse, and to estimate DOI positions by calculating ratios of these two measurements. This phosphor-coated crystal detector achieved a DOI resolution of about 8 mm. However, further improvements of DOI resolution for this design appear to be challenging because variations in the shapes of output pulses are large relative to differences between pulse shapes.

Another approach to the development of a cost-effective DOI PET detector involves the use of a monolithic crystal (scintillation crystal slab). Monolithic crystal detectors are cheaper than discrete crystal detectors because the large number of crystals required in discrete crystal arrays increase manufacturing costs. The monolithic crystal detector provides DOI information as a function of the extent of light dispersion (Tomitani *et al* 1999). In this detector, the performance of event positioning near the edges of a crystal slab is improved by incorporating a statistically based positioning (SBP) algorithm and by placing additional photosensors at the edges of the crystal (Joung *et al* 2002, Ling *et al* 2007). Currently, a detector module composed of a  $50 \times 50 \times 8$  mm<sup>3</sup> crystal and a 64-anode PMT provides a spatial resolution of at least 1.4 mm and 2 bits of DOI information (Lewellen 2008). However, the use of a thicker crystal to improve detection efficiency would cause positional distortion near the edges of the crystal. The stacking of multiple slabs (monolithic crystal layers) has been proposed as a solution to this problem, because this achieves high sensitivity while maintaining good positional resolution within a slab (Lewellen 2008). In this design, the use of PS-APDs or arrays of APDs or SiPMs would be desirable to detect events in each slab (Bruyndonckx *et al* 2007, Schaart *et al* 2009, Maas *et al* 2009).

For the majority of DOI estimation methods, DOI estimation accuracy deteriorates as the crystal length increases. A similar trend was observed in the present study, as shown in figure 5. The 2D variance maps estimated for various crystal sizes (figure 6) helped us understand the relationship between average DOI resolution and crystal size, as shown in figure 5. As shown in figure 5, DOI resolution was also found to be dependent on crystal cross-section and to improve as cross-section increases. In crystals with smaller cross-sections, variance values increase more slowly as DOI deviated from crystal centers possibly due to the larger number of optical interfaces per unit detector area.

The extent of light dispersion along crystals is mainly determined by two factors. The first is the amount of light cross-talk between two crystals, and this is greater for thinner crystals because of the greater surface/volume ratio. The second is the number of optical interfaces per unit detector area, which hinder light propagation, and this is also greater for thinner crystals. To investigate how these factors balance out when determining the extent of light dispersion, we performed additional optical simulations. LSO crystal arrays were modeled to yield the same total block area ( $\sim 12$  mm) as summarized in table 2, and light photons were generated at one center crystal in each crystal array.

The number of escaped photons from the first crystal where photons are produced (fourth column in table 2) and the total number of escaped photons from the array (fifth column) were determined at lateral crystal surfaces. The results obtained show that in thinner crystals

**Table 2.** Configurations of the crystal blocks used to investigate factors that influence the extent of light dispersion in a crystal array. The crystal length was fixed at 20 mm.

Crystal cross-sectional area (mm × mm)	Array size ( $n \times n$ )	Surface/volume ( $\text{mm}^2 \text{mm}^{-3}$ )	Escaped photons from the first crystal	Total escaped photons from the array
1.0 × 1.0	12 × 12	4.1	1710 (53.6%)	453 (14.2%)
1.5 × 1.5	8 × 8	2.8	1547 (48.5%)	610 (19.1%)
2.0 × 2.0	6 × 6	2.1	1449 (45.4%)	706 (22.1%)

a larger number of photons escape from the first crystal (probability because of the influence of the greater surface/volume ratio). However, the total number of escaped photons from the whole array was smaller for thinner crystals, indicating that the number of optical interfaces proportional to the array size (second column) predominantly determines the extent of light dispersion in this design.

The results of above simulation also suggest that DOI resolution can be more improved by modifying optical coupling between materials. In particular, the use of material with a refractive index appropriate for a given crystal size provides a possible means of controlling light dispersion. Furthermore, light dispersion could be controlled by reflector grids with different toothed shapes (i.e. trapezoid) or by applying a concentration gradient of reflecting paint on crystal surfaces.

Optical simulation helped us understand and verify the concept of new detector design and to optimize its design efficiently. Although the usefulness of GATE optical simulation for predicting detector characteristics has been demonstrated elsewhere (van der Laan *et al* 2010), it still has limitations in terms of providing quantitative information on some important detector parameters, such as, energy and timing resolutions, which are also influenced by PMTs and electric circuits. In the present study, we chose a fluctuating scale to the number of the photons to yield the real measurement value of 16% energy resolution to make the effects of statistical fluctuations and electronic noise reflected in the simulation results.

However, it should be noted that the individual channels of a multi-anode PMT have different QEs, gains, dark currents and readout electronics noises which were not taken into account in the present simulations. Furthermore, the timing resolution of a scintillation detector is difficult to predict solely by optical simulation, because this parameter is sensitive to the rising time and the transit-time jitter of PMTs and electronic noise.

Although the results of our simulation study show that excellent DOI resolutions can be obtained using our new DOI PET detector design, the question remains as to how good DOI resolution should be used to eliminate parallax errors effectively in real systems. In addition, considerable work needs to be done for implementing the current detector model to validate it based on comparisons to measurements and to explore other detector parameters, the latter of which are particularly important, because it does not make sense to optimize a detector only in terms of DOI resolution, especially if other important detector performance requirements are compromised.

## 5. Conclusion

The described DOI PET detector design provided DOI information as a function of direction and extent of 2D light dispersion within partially transparent crystal arrays. This was achieved by using a unique reflector grid structure with triangularly shaped toothed strips. The simulation studies performed demonstrated that our method provides excellent DOI resolution

and crystal separation, that is, a DOI resolution of 2.16 mm and a peak-to-valley ratio of 9:1 for a  $1.5 \times 1.5 \times 20$  mm<sup>3</sup> crystal array.

Furthermore, the described detector design has cost advantages because it only requires a mono-layer of unpolished crystals and a single-ended light readout. The single-ended readout scheme used is also suitable for building a full-ring PET system with minimal gaps between detector modules. In addition, a reduction in the number of electronic channels is possible by employing analog circuits to determine the centers and variances of light dispersion. Therefore, the detector design described in this study appears to have commercial potential and provides improved spatial resolution uniformity and detection sensitivity.

## Acknowledgments

This work was supported by grants from the Atomic Energy R&D Program (2008-2003852) and the Basic Research Program (2005-2004723) through the Korean Science and Engineering Foundation funded by the Korean Ministry of Education, Science and Technology.

## References

- Abreu M C *et al* 2006 Design and evaluation of the clear-PEM scanner for positron emission mammography *IEEE Trans. Nucl. Sci.* **53** 71–7
- Bruyndonckx P, Lemaître C, Schaart D, Maas M, Van Der Laan D J, Krieguer M, Devroede O and Tavernier S 2007 Towards a continuous crystal APD-based PET detector design *Nucl. Instrum. Methods. A* **571** 182–6
- Champley K M, Lewellen T K, MacDonald L R, Miyaoka R S and Kinahan P E 2008 Statistical three-dimensional positioning algorithm for high-resolution dMiCE PET detector 2008 *IEEE Nucl. Sci. Symp. Med. Imaging Conf. Record* pp 4751–4
- Derenzo S E, Moses W W, Jackson H G, Turko B T, Cahoon J L, Geyer A B and Vuletich T 1989 Initial characterization of a position-sensitive photodiode/BGO detector for PET *IEEE Trans. Nucl. Sci.* **36** 1084–9
- Du H, Yang Y, Glodo J, Wu Y, Shah K and Cherry S R 2009 Continuous depth-of-interaction encoding using phosphor-coated scintillators *Phys. Med. Biol.* **54** 1757–71
- GATE users guide v4.0.0. chapter 12.3.1 'UNIFIED model'
- Hong S J, Kwon S I, Ito M, Lee G S, Sim K S, Park K S, Rhee J T and Lee J S 2008 Concept verification of three-layer DOI detectors for small animal PET *IEEE Trans. Nucl. Sci.* **55** 912–7
- Jan S *et al* 2004 GATE: a simulation toolkit for PET and SPECT *Phys. Med. Biol.* **49** 4543–61
- Joung J, Miyaoka R S and Lewellen T K 2002 cMiCE: a high resolution animal PET using continuous LSO with a statistics based positioning scheme *Nucl. Instrum. Methods. A* **489** 584–98
- Kim J S, Lee J S, Im K C, Kim S J, Kim S Y, Lee D S and Moon D H 2007 Performance measurement of the microPET focus 120 scanner *J. Nucl. Med.* **48** 1527–35
- Kwon S I, Hong S J, Ito M, Yoon H S, Lee G S, Sim K S, Rhee J T, Lee D S and Lee J S 2008 Development of position encoding circuit for a multi-anode position sensitive photomultiplier tube *Nucl. Med. Mol. Imaging* **42** 469–77
- Lerche C W *et al* 2009 Depth of interaction detection for  $\gamma$ -ray imaging *Nucl. Instrum. Methods. A* **600** 624–34
- Levin A and Moisan C 1996 A more physical approach to model the surface treatment of scintillation counters and its implementation into DETECT 1996 *IEEE Nucl. Sci. Symp. Med. Imaging Conf. Record* vol 2 pp 702–6
- Lewellen T K 2008 Recent developments in PET detector technology *Phys. Med. Biol.* **53** R287–317
- Lewellen T K, Janes M and Miyaoka R S 2003 DMice—a depth-of-interaction detector design for PET scanners 2003 *IEEE Nucl. Sci. Symp. Med. Imaging Conf. Record* pp 2388–92
- Ling T, Lewellen T K and Miyaoka R S 2007 Improving the intrinsic spatial resolution performance of the continuous miniature crystal element (cMiCE) detector 2007 *IEEE Nucl. Sci. Symp. Med. Imaging Conf. Record* pp 4308–13
- Maas M C, Schaart D R, Van Der Laan D J, Bruyndonckx P, Lemaître C, Beekman F J and van Eijk C W E 2009 Monolithic scintillator PET detectors with intrinsic depth-of-interaction correction *Phys. Med. Biol.* **54** 1893–908
- Miyaoka R S, Kohlmyer S G and Lewellen T K 2001 Performance characteristics of micro crystal element (MiCE) detectors *IEEE Trans. Nucl. Sci.* **48** 1403–7

- Miyaoka R S and Lewellen T K 1998 Design of a depth of interaction (DOI) PET detector module *IEEE Trans. Nucl. Sci.* **45** 1069–73
- Moses W W 2001 Trends in PET imaging *Nucl. Instrum. Methods. A* **471** 209–14
- Moses W W, Derenzo S E, Melcher C L and Manente R A 1995 A room-temperature LSO/PIN photodiode pet detector module that measures depth of interaction *IEEE Trans. Nucl. Sci.* **42** 1085–9
- Orita N, Murayama H, Kawai H, Inadama N and Tsuda T 2005 Three-dimensional array of scintillation crystals with proper reflector arrangement for a depth of interaction detector *IEEE Trans. Nucl. Sci.* **52** 8–14
- Popov V, Majewski S and Welch B L 2006 A novel readout concept for multianode photomultiplier tubes with pad matrix anode layout *Nucl. Instrum. Methods A* **567** 319–22
- Schaart D R, vanDam H T, Seifert S, Vinke R, Dendooven P, Löhner H and Beekman F J 2009 A novel, SiPM-array-based, monolithic scintillator detector for PET *Phys. Med. Biol.* **54** 3501–12
- Seidel J, Vaquero J J, Siegel S, Gandler W R and Green M V 1999 Depth identification accuracy of a three layer phoswich PET detector module *IEEE Trans. Nucl. Sci.* **46** 485–90
- Shao Y, Silverman R W, Farrell R, Cirignano L, Grazioso R, Shah K S, Visser G, Clajus M, Tumer T O and Cherry S R 2000 Design studies of a high resolution PET detector using APD arrays *IEEE Trans. Nucl. Sci.* **47** 1051–7
- Streun M, Brandenburg G, Larue H, Saleh H, Zimmermann E, Ziemons K and Halling H 2003 Pulse shape discrimination of LSO and LuYAP scintillators for depth of interaction detection in PET *IEEE Trans. Nucl. Sci.* **50** 344–7
- Tomitani T *et al* 1999 Depth encoding of point-of-interaction in thick scintillation cameras *1999 IEEE Nucl. Sci. Symp. Med. Imaging Conf. Record* pp 1182–6
- Van Der Laan D J, Schaart D R, Maas M C, Beekman F J, Bruyndonckx P and Eijk C W E 2010 Optical simulation of monolithic scintillator detectors using GATE/GEANT4 *Phys. Med. Biol.* **55** 1659–1675
- Visser E P, Disselhorst J A, Brom M, Laverman P, Gotthardt M, Oyen W J and Boerman O C 2009 Spatial resolution and sensitivity of the Inveon small-animal PET scanner *J. Nucl. Med.* **50** 139–47
- Wang Y, Seidel J, Tsui B M, Vaquero J J and Pomper M G 2006 Performance evaluation of the GE healthcare eXplore VISTA dual-ring small-animal PET scanner *J. Nucl. Med.* **47** 1891–900
- Yang Y, Wu Y, Qi J, James S S, Du H, Dokhale P A, Shah K S, Farrell R and Cherry S R 2008 A prototype PET scanner with DOI-encoding detectors *J. Nucl. Med.* **49** 1132–40
- Zhang N, Thompson C J, Cayouette F, Jolly D and Kecani S 2003 A prototype modular detector design for high resolution positron emission mammography imaging *IEEE Trans. Nucl. Sci.* **50** 1624–9